PIER C

(Received 20 June 2023, Accepted 28 November 2023, Scheduled 24 December 2023)

Laser-Based Estimation of the Diffusion Coefficient Profile for the Karman Turbulence Spectrum in Heated Wind Tunnel Jets Using Genetic Algorithm Computation

Jacques Bernard Tissibe[1], Noé Richard Makon[1,3], Maurice Lamara[1], Elisabeth Ngo Nyobe[1,2], and Elkana Pemha[1,*]

[1] *Applied Mechanics Laboratory, Faculty of Science, University of Yaoundé I, P.O. Box 812, Yaoundé, Cameroon*
[2] *Department of Mathematics and Physical Science, National Advanced School of Engineering University of Yaoundé I, P.O. Box 8390, Yaoundé, Cameroon*
[3] *Department of Gazeous and Mechanical Engineering, National Advanced School of Mines and Petroleum Industries of Kaélé University of Maroua, P.O. Box 06, Kaélé, Cameroon*

ABSTRACT: Turbulence is a longstanding problem in fluid mechanics for which experimentation remains unavoidable. In contrast to conventional experimental techniques that inevitably require the introduction of probes into the flow, a very convenient technique would be one in which there is no contact between the measuring sensors and the flow. The laser-based diagnostic technique reported in this work is described as an estimation of a large number of parameters defining the diffusion coefficient profile in the heated turbulent wind tunnel jet, which is required in the formula of the Karman turbulence spectrum for the jet under study. For this purpose, some required experiments in the jet are carried out. A laser beam is then sent perpendicular to the jet exhaust, and measurements of the probabilities of the position of the laser beam's impact on a photocell placed outside the jet are performed. Using the Markovian model, the same probabilities are calculated numerically. For these numerical results to agree with the experimental results, a numerical optimal-control strategy is applied. Due to the large number of unknown parameters searched, a genetic algorithm (GA) computation is performed. A good agreement observed between the GA results and those derived from the previously published cold-wire-anemometer data, combined with the use of the Dale-Gladstone law, proves the validity and accuracy of the laser-based genetic measurement technique.

1. INTRODUCTION

Turbulence is a longstanding problem in fluid mechanics for which experimentation remains unavoidable, and the conventional experimental techniques that are usually employed need inevitable probes to be introduced into the flow. A very convenient technique would be one in which there is no contact between the measuring sensors and the flows, and diagnostic techniques are then increasingly used. This paper is devoted to a laser-based diagnostic technique including an inverse problem whose solution, obtained from an optimal-control approach, is the profile of a parameter needed in the formula of the Karman turbulence spectrum for a heated turbulent wind tunnel jet.

In the previous papers of our research team [1, 2], an experiment using laser beam propagation in the jet considered and similar to the one presented in this paper was carried out to extract an important coefficient called the diffusion coefficient. In [1, 2], the measured diffusion coefficient was constant because the laser ray was sent parallel to the jet exhaust.

As in the previous works [1, 2], this paper is also devoted to the determination of the diffusion coefficient, but the foundational difference between this work and the previous ones lies on two levels. First, in this paper, the laser beam is sent perpendicularly to the jet exhaust so that the diffusion coefficient is a variable parameter along the path of the laser ray. So, the solution sought is more complicated because it represents the profile of the diffusion coefficient. Second, genetic algorithms have been previously used in [1, 2] to determine the coefficients of Fourier expansion for the modeling of the laser ray direction, whereas in this paper, they are applied to directly find the profile of the diffusion coefficient.

To perform the measurement technique presented in this work, experimental and numerical means are required. On the experimental level, with the jet that is heated, the mean temperature, mean velocity, and rms of temperature fluctuations are measured along a direction, which is perpendicular to the jet exhaust and is the direction given to the laser ray during its propagation in the jet under study. In addition, measurements of the probabilities of the positions of the laser beam's impact on a photocell placed outside the jet are required.

On the numerical level, the same probabilities are computed from the second Kolmogorov equation provided by the Markovian process model, which is applied along the whole path of the laser ray. The profile of the diffusion coefficient is then determined using an optimal control approach that reduces to the minimum, a cost function defined as the quadratic difference between numerical and experimental probabilities. Due to the large number of parameters searched, the use of a genetic algorithm is recommended. The good agreement between

* Corresponding author: Elkana Pemha (elkanaderbeau@yahoo.fr).

our results and those deduced from the published cold-wire anemometer data, combined with the application of the Dale-Gladstone (DG) law, demonstrate the validity of the laser-based diagnostic technique.

For a better understanding of the present work, this paper is organized into seven sections: Section 2 is devoted to theory and shows how the Karman turbulence spectrum depends on the diffusion coefficient. In Section 3, experimental tools that are required for the diagnostic technique are used. Computation tools for this technique are applied in Section 4. In Section 5, the optimal-control strategy using genetic algorithm is described in detail. The results obtained are presented, and their validation is proved in Section 6. The paper ends by Section 7 that serves as a conclusion.

2. KARMAN TURBULENCE SPECTRUM IN TERMS OF THE DIFFUSION COEFFICIENT

Chernov demonstrated, for the first time [3], that the variance of deflection angle ε of the light ray after having traversed a distance X in the jet is proportional to X, according to the formula,

$$\overline{\varepsilon^2} = \frac{4}{(\bar{n})^2} D_\mu X, \tag{1a}$$

where $\bar{n}$ represents the mean value of refractive index n, and D_μ is a crucial parameter called diffusion coefficient of the turbulent jet and defined as:

$$D_\mu = -\frac{\overline{\mu^2}}{2} \int_0^\infty \Delta R_\mu(0, r, 0) dr. \tag{1b}$$

In Equation (1b), Δ represents the Laplacian operator, and R_μ stands for the correlation coefficient of the refractive index fluctuations μ that are evaluated at two points located on the path of the light ray.

On the other hand, it is known that Karman's model of turbulence spectrum is given by the relation [4]:

$$\phi_\mu(K) = 0.033 C_\mu^2 \left(K^2 + K_0^2\right)^{-11/6} \exp\left(-K^2/K_m^2\right), \tag{2}$$

where C_μ^2 is the structure coefficient of the refractive index fluctuations, and K_0 and K_m are the lower and upper limits of the turbulence inertial zone ($K_0 = 0.1\,\mathrm{mm}^{-1}$; $K_m = 5.92\,\mathrm{mm}^{-1}$ [1, 2]).

As done in our previous work [5], we proved that there exists a relationship that connects the coefficients D_μ and C_μ^2. For this purpose, we found that the correlation function $R_{\varepsilon\varepsilon}$ of deflection angles of the laser beam, which is evaluated at the two points separated by a transverse distance ρ and located on the detection plane at a distance X from the entry border of the jet, is given by the following relation [5]:

$$R_{\varepsilon\varepsilon}(X, \eta) = \frac{0.264\pi}{(\bar{n})^2} C_\mu^2 K_m^{1/3} X \left| \int_0^\infty \phi(\xi, \eta) d\xi \right|, \tag{3a}$$

with $\phi(\xi, \eta)$ given as:

$$\phi(\xi, \eta) = \int_0^\infty \sigma \left(\sigma^2 + \sigma_0^2\right)^{-11/6} \exp\left(-\sigma^2\right) \left[\left(\frac{\sigma^2\eta^2 + 2}{p^3} - \frac{3\eta^2}{p^5} \right) \sin(p\sigma) + \left(\frac{3\sigma\eta^2}{p^4} - \frac{2\sigma}{p^2} \right) \cos(p\sigma) \right] d\sigma \tag{3b}$$

where η, p, and σ are dimensionless variables defined as: $\eta = K_m\rho$, $p = \sqrt{\xi^2 + \eta^2}$, $\sigma = K/K_m$, and $\sigma_0 = K_0/K_m$. Using the identity, $\overline{\varepsilon^2} = R_{\varepsilon\varepsilon}(X, \eta = 0)$, we deduce an equivalent expression of the variance $\overline{\varepsilon^2}$ from the correlation function given in Equation (3a):

$$\overline{\varepsilon^2} = \frac{0.264\pi}{(\bar{n})^2} C_\mu^2 K_m^{1/3} X \left| \int_0^\infty \psi(\xi) d\xi \right|, \tag{4}$$

where the function $\psi(\xi)$ is defined from Equation (3b) as follows:

$$\psi(\xi) = \phi(\xi, \eta = 0) = \int_0^\infty \sigma \left(\sigma^2 + \sigma_0^2\right)^{-11/6} \exp\left(-\sigma^2\right) \left[\frac{2}{\xi^3} \sin(\xi\sigma) - \frac{2\sigma}{\xi^2} \cos(\xi\sigma) \right] d\sigma. \tag{5}$$

Comparing our results obtained in Equation (4) to those given by the Chernov law in Equation (1a), we obtain the relationship between the structure coefficient (C_μ^2) and diffusion coefficient (D_μ), which was found in our previous work [5]:

$$C_\mu^2 = D_\mu \left(0.066\pi K_m^{1/3} \left| \int_0^\infty \psi(\xi) d\xi \right| \right)^{-1}. \tag{6}$$

Using Equations (2) and (6), the Karman turbulence spectrum is written in terms of D_μ as:

$$\phi_\mu(K) = 0.033 D_\mu \left(0.066\pi K_m^{1/3} \left| \int_0^\infty \psi(\xi) d\xi \right| \right)^{-1} \left(K^2 + K_0^2\right)^{-11/6} \exp\left(-K^2/K_m^2\right). \tag{7}$$

3. EXPERIMENTAL TOOLS FOR THE DIAGNOSTIC TECHNIQUE

3.1. Wind Tunnel

Figure 1 shows the wind tunnel that provides a hot turbulent jet of air from a nozzle.

3.2. Measurements Required

The experimental setup is shown schematically in Figure 2. A red light ray created from a 5 mW He-Ne laser and having wavelength $\lambda = 6328$ A, initial diameter $a_0 = 0.8$ mm, and spectral width $\Delta\lambda = 6.4 \times 10^{-4}$ A is passed through the heated wind tunnel jet before reaching a photocell placed outside the jet at a distance $d = 500$ mm. The amplitude of the electrical signal transmitted by the photocell is very weak, and it is necessary to use an amplifier which gives information to an interface

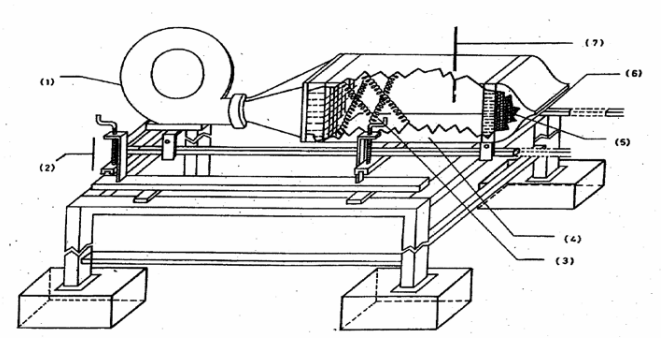

FIGURE 1. Complete anatomy of the wind tunnel providing the heated turbulent jet: (1) Ventilating fan; (2) Vertical displacement; (3) Heating resistances; (4) Box for flow homogeneity; (5) Filter against turbulence; (6) Nozzle (200 mm × 5 mm); (7) Thermocouple.

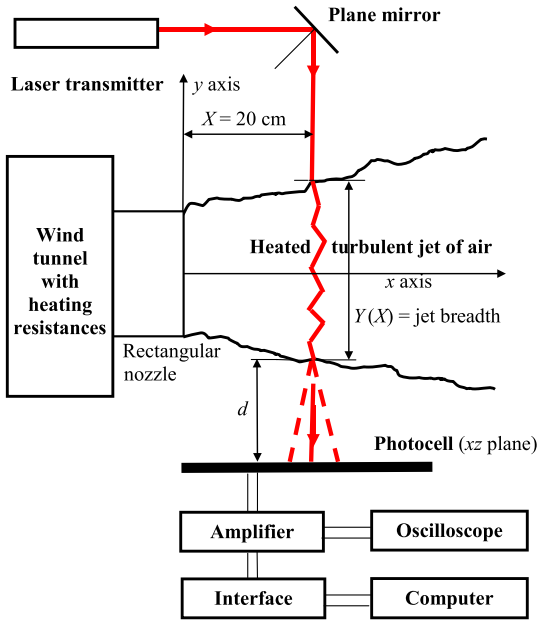

FIGURE 2. Experimental setup.

connected to a computer for statistical investigations. To keep the position of the laser source unchanged when seeking the incident direction of the laser ray, we need to use a plane mirror, as seen in Figure 2. This figure also shows the three Cartesian perpendicular axes (x, y, z) defined on the nozzle aperture with the origin at the centre of the aperture. Before entering the jet, the laser ray is placed in the median plane $z = 0$ of the nozzle aperture, along the direction parallel to the y axis and located at a distance $X = 200$ mm from the plane of the nozzle aperture. The mean distance traversed by the laser ray is nearly equal to the jet breadth $Y = 100$ cm (see Figure 2).

The cell plane is cross-ruled in 1600 small squares of same size $c = 0.01$ cm such that:

$$x(l) = x_0 + l \cdot c,\ l = 0, 1, ..., L,\ (L = 40), \quad \text{with } x_0 = -0.20\,\text{cm}, \tag{8a}$$

$$z(m) = z_0 + m \cdot c,\ m = 0, 1, ..., M,\ (M = 40), \quad \text{with } z_0 = -0.20\,\text{cm} \tag{8b}$$

In the absence of the jet, we verify that the ambient medium at rest has no influence in the laser ray propagation because its trajectory remains rectilinear. In that case, the two voltages derived from the photocell are adjusted to be equal to zero, and the corresponding laser ray impact is taken as the origin of the cell plane, at the point whose l and m are given by: $l = i = 22$ and $m = j = 19$. The diameter of the laser ray footprint is equal to 0.85 mm and represents 21% of the size of the final measuring square. The surface of this footprint is equal to 0.384 mm^2 and represents 3.5% of the surface of the final measuring square.

The probability for the laser ray impact to be located in the small photocell square $[x(l), x(l+1) \times z(m), z(m+1)]$ is represented by $W(l, m)$ and is plotted in Figure 3. The luminous trace produced by the laser ray on the photocell plane is presented in Figure 4.

We have used $2 \times (2^6 \times 2^6) = 8192$ impacts of the laser ray on the detector in approximately 20 seconds. This number of impacts is the maximum allowed by the interface apparatus.

Measurements of the mean velocity and temperature are carried out along the direction given to the laser ray by means of the apparatus described in [1, 2]. The values obtained are plotted in Figure 5. The mean-velocity plot shows that the distance of the path traversed by the laser ray in the jet is $Y = 100$ cm and is located between the values $y = \pm 50$ cm.

We measure the variance of temperature fluctuations (see Figure 6), by means of the cold-wire anemometer technique [6], which utilizes a wire having diameter and length equal to 1 µm and 0.5 mm, respectively, with a current intensity $I_0 = 0.15$ mA.

Let us deduce the values of the variance of refractive index fluctuations from those of the variance of temperature fluctuations. For this purpose, we assume that the jet air may be considered as a perfect gas. According to the Dale-Gladstone (DG) law [7], the refractive index n at any point of the jet is connected to the pressure (P_{jet}) and temperature (T_{jet}) at the point considered by the following relationship:

$$n = 1 + \frac{G(\lambda) P_{\text{jet}}}{r_0 T_{\text{jet}}}, \tag{9}$$

where $G(\lambda)$ is the DG constant that depends on the radiation wavelength λ, and r_0 is the specific constant of the perfect gas. For the laser ray we have used, the incident wavelength is $\lambda_0 = 6328$Å, and the corresponding value of the parameter a_0, defined as: $a_0 = G(\lambda)/r_0$, is 79×10^{-6} K·mb^{-1}.

Differentiating Equation (9), one obtains:

$$dn = -\left(\frac{a_0 P_{\text{jet}}}{T_{\text{jet}}^2}\right) dT_{\text{jet}} + \left(\frac{a_0}{T_{\text{jet}}}\right) dP_{\text{jet}}. \tag{10}$$

Before the jet is heated, we note in the course of our experimentation that the path of the laser ray in the jet remains almost rectilinear. We then deduce that the laser ray trajectory in the jet is nearly rectilinear in the absence of temperature fluctuations. This leads to concluding that $dP_{\text{jet}} \approx 0$, that is, the pressure fluctuations may be neglected in the jet considered and that the temperature fluctuations are the unique cause of the fluctuations undergone by the refractive index in the heated jet under

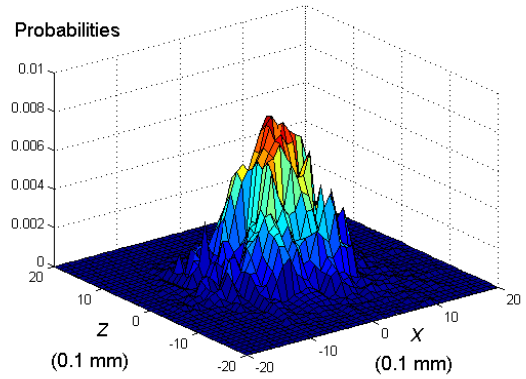

FIGURE 3. Experimental probabilities of position of the laser ray impact on the photocell.

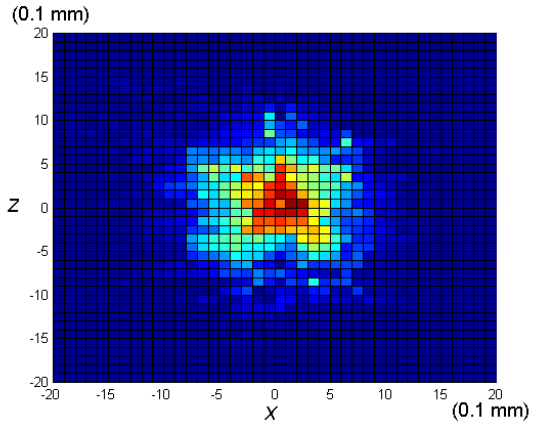

FIGURE 4. Luminous trace produced by the laser ray impact on the photocell plane.

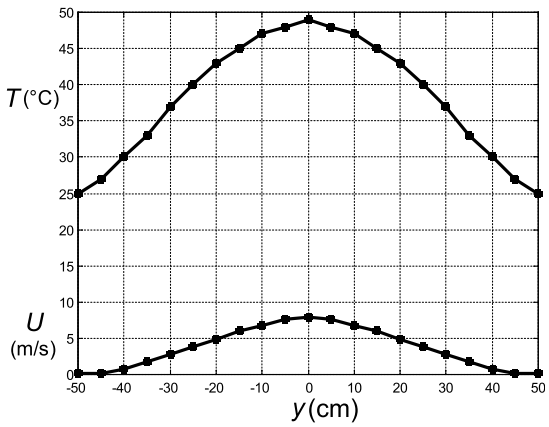

FIGURE 5. Mean temperature and mean velocity along the path of the laser ray in the jet.

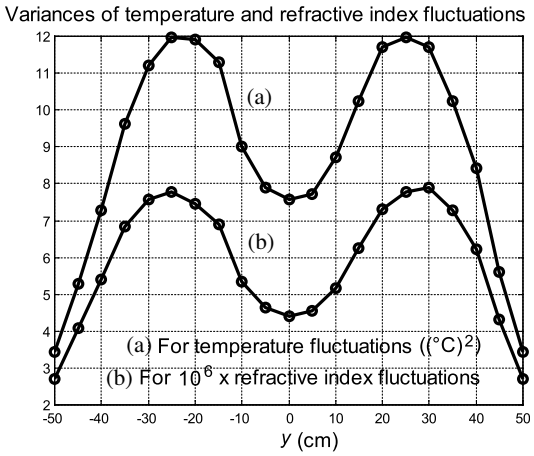

FIGURE 6. Variance along the mean path of the laser ray for (a) temperature fluctuations $((^\circ\mathrm{C})^2)$ and for (b) refractive index fluctuations $\times 10^6$.

study. In addition, we have $T_{\text{jet}} = T + \theta$ where T represents the mean temperature, and θ stands for the temperature fluctuation, which is very small compared to T. Considering the small finite differences θ and μ in the place of dT_{jet} and dn, respectively, we obtain the simplified form of Equation (10), $\mu = -(a_0 P_0/T^2)\theta$, where $P_{\text{jet}} = P_0 = 1000\,\text{mb}$ is the value of the constant air pressure. One then deduces the relationship between μ and θ, along the y-axis considered as the mean path of the laser ray:

$$\overline{\mu^2}(y) = \left(\frac{a_0 P_0}{T^2(y)}\right)^2 \overline{\theta^2}(y). \tag{11}$$

Equation (11) enables one to calculate the variance of refractive index fluctuations using the measured values of the variance of temperature fluctuations together with the values obtained for the measurement of the mean temperature, $T = T(y)$. The values thus obtained are plotted in Figure 6 as a function of the propagation distance of the laser ray.

4. COMPUTATION TOOLS FOR THE DIAGNOSTIC TECHNIQUE

4.1. Markov Process Model along the Laser Ray Path Perpendicular to the Jet Exhaust

As suggested by Chernov [3], the random direction of the laser ray can be regarded as a Markov process in which the probability $P(\phi, \theta, \sigma)$ for the laser ray to have the direction defined by the angles (ϕ, θ) (ϕ is the polar angle and θ the azimuthal) after going a distance σ in the jet, satisfies the Einstein-Fokker-Kolomogrov (EFK) equation [8]. With the deflection angle of the laser ray being small, we set $\sigma \approx y$ and obtain the approximate EFK equation:

$$\frac{\partial P}{\partial y} = \frac{D_\mu(y)}{\sin\theta}\frac{\partial}{\partial\theta}\left(\sin\theta\frac{\partial P}{\partial\theta}\right) + \frac{D_\mu(y)}{\sin^2\theta}\frac{\partial^2 P}{\partial\phi^2}, \tag{12a}$$

with the zero boundary condition and the initial condition given by:

$$P(\phi, \theta, y = y_0) = \delta(\phi)\delta(\theta - \pi/2), \tag{12b}$$

where δ represents the Dirac distribution, and $(\phi = 0, \theta = \pi/2)$ are the angles of the laser ray direction before entering the jet at the point $y = y_0$.

4.2. Discretization Scheme for Equation (12a)

The solution $P(\phi, \theta, y)$ of Equation (12a) is approximated as $P(\phi_l, \theta_m, y_n) = P^n(l, m)$, where ϕ_l, θ_m, and y_n represent the discretization values to be determined for ϕ, θ, and y, respectively. Using the relations we found in [1, 2] and exploiting Equations (8a) and (8b), we compute these values (ϕ_l, θ_m) so that the probabilities $P(\phi_l, \theta_m, y_n)$ are replaced with $P(x(l), z(m), y(n))$, which define the probabilities of the position $(x(l), z(m))$ of the laser ray impact on the photocell plane. For the values y_n, we adopt a constant step a whose value $a = 5\,\text{mm}$ is obtained from the convergence of the numerical scheme we have applied.

To solve Equation (12a), we adopt an explicit discretization scheme [9] with alternating-directions, in which the initial condition (Equation (12b)) is discretized in terms of Kronecker delta as follows:

$$P(\phi, \theta, y = y_0) = P^{n=0}(l, m) = \delta(l, i)\delta(m, j), \qquad (13)$$

where i and j are the integers that define the origin of the experimental measuring square ($i = 22$; $j = 19$).

5. MEASUREMENT OF THE DIFFUSION COEFFICIENT PROFILE USING GENETIC ALGORITHM (GA)

5.1. Construction of the Cost Function

With a view to comparing the experimental probabilities $W(l, m)$ to the corresponding numerical results $P(l, m, N) = P^N(l, m)$ obtained at the photocell plane, we define a cost function J, which measures the quadratic difference between the two sets of probabilities and depends on the diffusion coefficient profile $D_\mu(y)$ as follows:

$$J(D(y)) = \sum_{l=0}^{L} \sum_{m=0}^{M} \left(P^N(l, m, D_\mu(y)) - W(l, m)\right)^2 \qquad (14)$$

The cost function, J, depends on N parameters (D^n) that represent the values of the diffusion coefficient given in its profile, with $n = 1, 2, ..., N$ and $N = Y/a = 20$. We note that the numerical procedure does not need the value (D^0) of the diffusion coefficient at the entry point of the jet. This value will be found by applying stochastic extrapolation. Minimizing J is well known as an inverse problem of the parameter estimation type [10]. The GA is strongly recommended for this problem because J depends on a large number of parameters having an unknown connection with J. As the local minimum of J is also its global minimum due to the form of Equation (14) defining the cost function, the problem under study can also be solved using a convex programming algorithm [11].

5.2. General Structure of a GA

The GAs were first introduced by Holland [12] and extensively developed by Goldberg [13] and Deb [14]. A GA works with a population of candidate solutions that are called individuals. It initializes a sample population, and this population changes over generations with an unchanged number of individuals. Each individual is represented by a code defined by a single string of characters called chromosomes. A positive fitness function whose definition does not depend on generation enables one to calculate, at each generation, the fitness of the current individuals. Based on the genetics of the human being's evolution, that is, the evolution via the survival of the fittest, a new generation of individuals is generated after the three genetic operators: selection, crossover, and mutation.

5.3. About the GA We Have Constructed

Since we have found that the order of magnitude of the cost function is $J \approx 10^{-4}$, we define the fitness function as $F = 1.0 - \alpha J$, such that maximizing F means minimizing J. The parameter $\alpha = 10$ is used to make the discrepancies between the values of F significant.

To code individuals, we need to know the exploration area of the parameters to be optimized. From the genetic point of view, this exploration area should be large enough to avoid a priori exclusion of potential solutions, and this could include some "bad individuals" in order to create a diverse population, which helps to avoid premature convergence of the GA. As the order of magnitude of the diffusion coefficient for the jet studied is equal to $10^{-9}\,\text{m}^{-1}$ [1, 2], we take the exploration area that is defined by the interval $[D_{\text{min}}, D_{\text{max}}]$ with $D_{\text{min}} = 10^{-9}\,\text{m}^{-1}$ and $D_{\text{max}} = 10.0 \times 10^{-9}\,\text{m}^{-1}$. To code each parameter (D^n), we discretize it as a set of Q possible values that are denoted by $(D^n)_q$ such that:

$$(D^n)_q = D_{\text{min}} + q\left((D_{\text{max}} - D_{\text{min}})/(Q-1)\right), \quad \text{for } q = 0, 1, ..., Q-1 \text{ and } n = 1, ..., N \qquad (15)$$

We then apply a binary code. In this regard, relation (15) shows that there is a unique correspondence between each value $(D^n)_q$ and the discretization integer q such that coding $(D^n)_q$ means coding the integer q. With the maximum value of q being $Q - 1$, the number R of bits needed for this coding must satisfy the condition: $Q - 1 \leq 2^R - 1$, that is, $Q \leq 2^R$. For simplicity, we then adjust the number Q of discretization values to a power of 2, and we adopt $Q = 2^7 = 128$, that is, 7 chromosomes per parameter. So, each individual is encoded as the concatenation of 20 groups of 7 chromosomes, giving a string of 140 chromosomes.

Knowing the total number of bits and applying bits 0 or 1, the initial population is stochastically generated. The selection technique applied is tournament selection [12–14] with shuffling like in domino games. To improve the convergence of our GA, we have applied the "elitist strategy," which requires the fittest individual of each generation to survive into the next generation. The GA is implemented using random-site crossovers with a rate of 0.70, genotypic mutations with a rate of 0.02, and phenotypic mutations with a rate of 0.04. To end the work of our GA, we adopt the usual criterion, which consists of fixing arbitrarily the number of generations beforehand. Usually, one hopes that the GA will converge before reaching the end of the

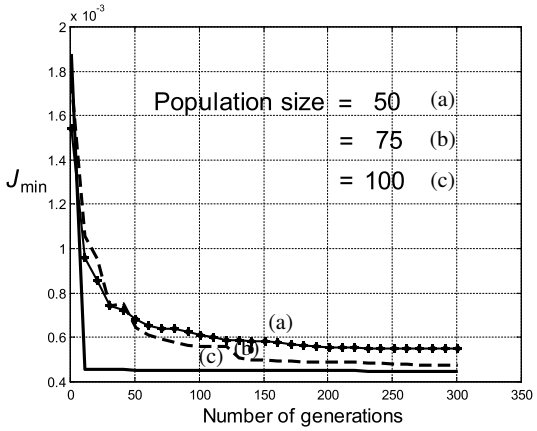

FIGURE 7. Convergence history of the GA for the population size: (a) 50; (b) 75; (c) 100.

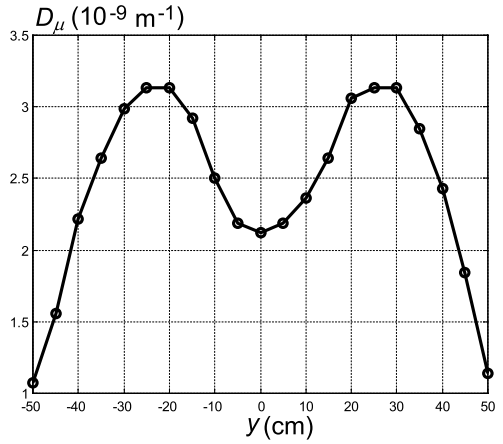

FIGURE 8. Optimum profile of the diffusion coefficient D_μ found from the GA.

TABLE 1. Code of the best individual given by the GA.

0	0	0	0	0	0	1	0	0	0	1	0	0
0	0	0	1	0	0	1	0	0	0	1	1	0
0	0	0	0	1	1	1	0	1	0	0	1	1
1	1	1	0	0	1	1	1	1	1	0	0	1
1	1	0	0	0	0	1	0	1	1	0	0	0
1	0	0	0	1	0	0	1	0	0	0	0	0
0	1	0	0	0	1	0	0	1	0	1	0	0
0	0	1	1	0	0	0	0	0	1	1	1	1
0	0	0	1	1	1	1	1	0	0	1	1	1
1	1	0	0	1	1	0	1	1	0	0	1	0
1	0	1	0	0	0	1	1	0	0	0	0	0
0	0	1	0									

process. The number of generations arbitrarily adopted is equal to 300.

6. RESULTS AND VALIDATION

6.1. GA Iteration History

Figure 7 shows the convergence history of the GA for the population size (50, 75, 100). As the minima found for J are $J_{\min} = 5.51 \times 10^{-4}$, 4.73×10^{-4}, and 4.48×10^{-4}, respectively, we retain the value $J_{\min} = 4.48 \times 10^{-4}$ obtained for the population size equal to 100. With this population, the GA begins to converge after 241 generations, when the best individual for all subsequent generations is obtained for the first time.

6.2 Code of the Best Individual and Diffusion Coefficient Profile Given by the GA

The code of this best individual is presented in Table 1, as a string of 147 chromosomes, with the first group of 7 chromosomes being added for (D^0). Decoding this best individual, we obtain the optimum profile of the diffusion coefficient, $D_\mu = D_\mu(y)$, which we present in Figure 8.

6.3. Validation of the GA Results

As seen in Figure 8, the value of D_μ at the median point $y = 0$ is $D_\mu = 2.12 \times 10^{-9}\,\mathrm{m}^{-1}$. This result is close to the value $D_\mu = 2.98 \times 10^{-9}\,\mathrm{m}^{-1}$ obtained at $y = 0$ for the same jet, in a previous work of our research team [15], when determining the constant diffusion coefficient along the z-axis using the gradient-descent optimization.

To rigorously validate the results obtained from the GA, we find that the diffusion coefficient is connected to another coefficient D_θ by the following relationship derived from Equation (11):

$$D_\mu = \left(\frac{aP_0}{T^2}\right)^2 \overline{\theta^2} D_\theta, \tag{16}$$

where $\overline{\theta^2}$ stands for the variance of temperature fluctuations. The parameter D_θ was introduced for the first time in [16] and defined as:

$$D_\theta = -\frac{1}{2}\int_0^\infty \Delta R_\theta(0, r, 0)dr, \tag{17}$$

where R_θ represents the correlation coefficient of temperature fluctuations and Δ the Laplacian operator.

We need to compare the optimal profile $D_\mu(y)$, which is derived from the GA and plotted in Figure 8, to the profile $D_\mu(y)$

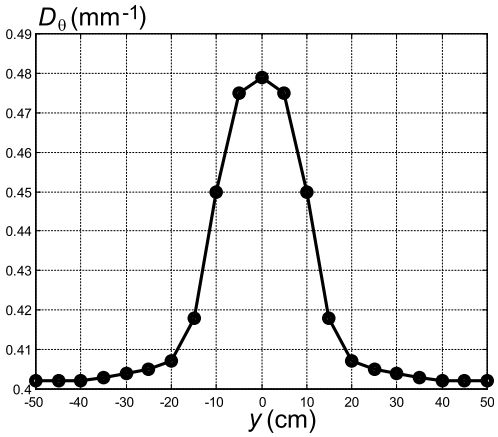

FIGURE 9. Values of the parameter D_θ measured by Gagnaire and Tailland [16] and plotted as a function of the laser ray propagation distance perpendicular to the nozzle aperture.

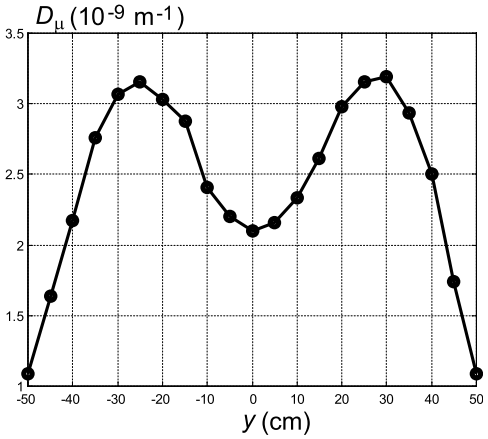

FIGURE 10. Profile $D_\mu(y)$ obtained from Equation (16) using the measured values of the mean temperature T and temperature fluctuations $\overline{\theta^2}$, together with the values of $D_\theta(y)$ that were measured in Ref. [16].

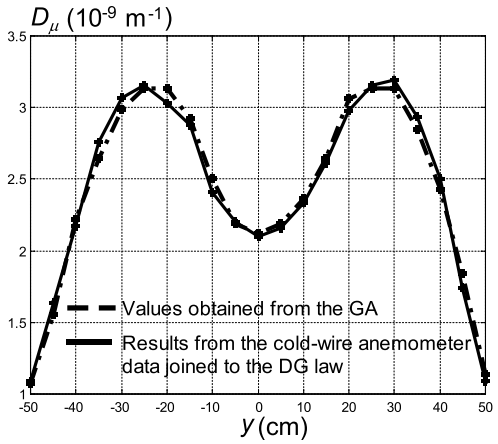

FIGURE 11. Comparison between the diffusion coefficient profile obtained from the GA and that calculated using the cold-wire anemometer data joined to the DG law.

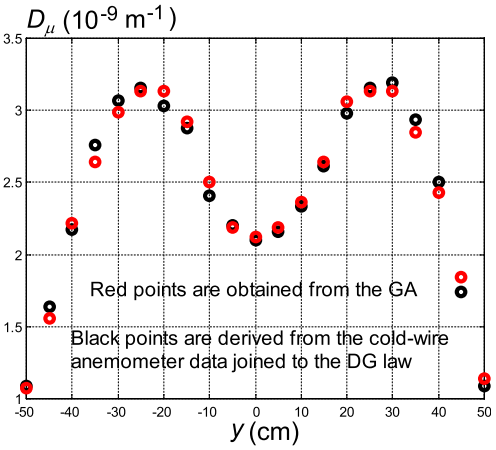

FIGURE 12. Point-by-point comparison between the diffusion coefficient profile obtained from the GA and that calculated using the cold-wire anemometer data joined to the DG law.

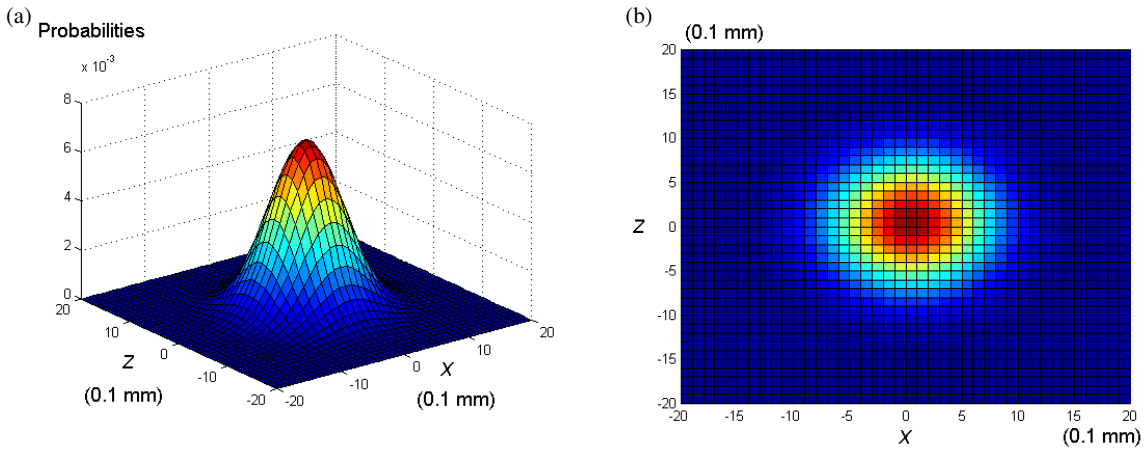

FIGURE 13. Markovian-hypothesis predicted results for (a) the probabilities of the position of the laser ray impact on the photocell placed outside the jet and (b) the luminous trace produced by the laser ray impact on the photocell.

that is computed from Equation (16), if the values of D_θ, T, and $\overline{\theta^2}$ as a function of y are known. For this purpose, we use the experimental values of T and $\overline{\theta^2}$ that we have measured and plotted in Figures 5 and 6, respectively. In addition, we exploit the values of D_θ measured in [16] by means of the cold-wire anemometer and presented in Figure 9. The values of D_μ ob-

tained from Equation (16) form a profile that is plotted in Figure 10.

The comparison between the values of $D_\mu(y)$ obtained from the GA and those calculated using Equation (16) is performed and presented in Figures 11 and 12. Figure 11 shows the profiles of the two sets of results, and Figure 12 highlights the point-by-point comparison of these results.

In Figures 11 and 12, a good agreement is observed between the GA optimum profile of the diffusion coefficient and that obtained from the cold-wire-anemometer data with the use of the Dale-Gladstone law.

The Markovian-hypothesis predicted values $P^n(l,m)$ obtained as the numerical solution of Equation (12a) using the GA optimum profile of the diffusion coefficient are plotted in Figure 13(a), and the corresponding luminous trace of the laser ray on the photocell plane is shown in Figure 13(b). These figures must be compared to the experimental ones, which are presented in Figures 3 and 4.

Due to the good agreement between experimental and GA results, one can confirm that the Markovian hypothesis, which was suggested for the first time by Chernov [3] to predict the propagation of a light ray in a random medium such as the turbulent jet under study, represents a satisfactory model. Of course, this model holds when the geometrical optics approximation is valid, that is when it is allowed to ignore the diffraction effects that could occur during the propagation of the laser ray in the jet studied.

7. CONCLUSION

This study is devoted to a laser-based diagnostic technique for solving an engineering inverse problem using a genetic algorithm with an optimal-control strategy. The objective is to achieve an estimation of a large number of parameters, thereby defining the diffusion coefficient profile required in the formula of the Karman turbulence spectrum for a heated turbulent wind tunnel jet. To perform this diagnostic technique, experimental and computational tools that are needed are described in detail. A good agreement is observed between the GA optimum profile and the profile obtained from the cold-wire-anemometer data combined with the use of the Dale-Gladstone law.

REFERENCES

[1] Ngo Nyobe, E. and E. Pemha, "Shape optimization using genetic algorithms and laser beam propagation for the determination of the diffusion coefficient in a hot turbulent jet of air," *Progress In Electromagnetics Research B*, Vol. 4, 211–221, 2008.

[2] Pemha, E. and E. Nyobe, "Genetic algorithm approach and experimental confirmation of a laser-based diagnostic technique for the local thermal turbulence in a hot wind tunnel jet," *Progress In Electromagnetics Research B*, Vol. 28, 325–350, 2011.

[3] Chernov, L. A., *Wave Propagation in a Random Medium*, McGraw-Hill, New York, 1960.

[4] Hinze, J. O., *Turbulence: An Introduction to Its Mechanisms and Theory*, McGraw-Hill, New York, 1976.

[5] Jean Bilong, I., E. Nyobe, J. Hona, and E. Pemha, "Correlations of deflection angles of a laser beam in a hot turbulent jet of air: Theoretical determination and experimental measurement of the structure coefficient of refractive index fluctuations," *Progress In Electromagnetics Research B*, Vol. 42, 425–453, 2012.

[6] Comte-Bellot, G., "Hot-wire anemometry," *Annual Review of Fluid Mechanics*, Vol. 8, 209–231, 1976.

[7] Tatarskii, V. I., *The Effects of the Turbulent Atmosphere on Wave Propagation*, Jerusalem: Israel Program for Scientific Translations, 1971.

[8] Levine, B., *Fondements Théoriques de la Radiotechnique Statistique*, Editions Mir, Vol. 1, Moscou, 1973.

[9] Mitchell, A. R., *Computational Methods in Partial Differential Equations*, John Wiley and Sons, New York, 1974.

[10] Beck, J. V. and K. J. Arnold, *Parameter Estimation in Engineering and Science*, John Wiley and Sons, New York, 1977.

[11] Morabito, A., R. Palmeri, V. A. Morabito, A. Laganà, and T. Isernia, "Single-surface phaseless characterization of antennas via hierarchically ordered optimizations," *IEEE Transactions on Antennas and Propagation*, Vol. 67, No. 1, 461–474, Jan. 2019.

[12] Holland, J. H., *Adaptation in Natural and Artificial Systems*, University of Michigan Press, Ann Arbor, 1975.

[13] Goldberg, D. E., *Genetic Algorithms in Search, Optimization and Machine Learning*, Addison-Wesley, Reading, MA, 1989.

[14] Deb, K., *Multi-objective Optimization Using Evolutionary Algorithms*, John Wiley and Sons, New York, 2001.

[15] Pemha, E., B. Gay, and A. Tailland, "Measurement of the diffusion-coefficient in a heated plane airstream," *Physics of Fluids A-Fluid Dynamics*, Vol. 5, No. 6, 1289–1295, Jun. 1993.

[16] Gagnaire, A. and A. Tailland, "Interferometrical setup for the study of thermic turbulence in a plane airstream," *Proceedings of SPIE - The International Society for Optical Engineering*, Vol. 136, 69–73, 1978.